Clusterization and Strong Coupled-Channels Effects in Deuteron Interaction with ^{9}Be Nuclei

B A Urazbekov[1,2,3,4], A S Denikin[2,4], S M Lukyanov[4], N Itaco[1,3], D M Janseitov[4,5], K Mendibayev[4,6,7], V Burjan[8], V Kroha[8], J Mrazek[8], W H Trzaska[9], M N Harakeh[10], D Etasse[11], I Stefan[12], D Verney[12], T Issatayev[4,6], Yu E Penionzhkevich[4], K A Kuterbekov[6] and T Zholdybayev[5,7]

[1] Dipartimento di Matematica e Fisica, Università degli Studi della Campania Luigi Vanvitelli, I-8110 Caserta, Italy
[2] Dubna State University, 141982 Dubna, Russia
[3] Istituto Nazionale di Fisica Nucleare, Complesso Univeristario di Monte S. Angelo, I-80126 Napoli, Italy
[4] Joint Institute for nuclear research, 141980 Dubna, Russia
[5] Al-Farabi Kazakh National University, 050040 Almaty, Kazakhstan
[6] L N Gumilyov Eurasian National University, 010008 Nur-Sultan, Kazakhstan
[7] Institute of Nuclear Physics, 050032 Almaty, Kazakhstan
[8] Nuclear Physics Institute CAS, 25068 Řež, Czech Republic
[9] Department of Physics, University of Jyväskylä, FIN-40014 Jyväskylä, Finland
[10] KVI-CART, University of Groningen, 9747 AA Groningen, The Netherlands
[11] Normandie Université, ENSICAEN, UNICAEN, CNRS/IN2P3, LPC Caen, 14000 Caen, France
[12] Institut de Physique Nucléaire, Univ. Paris-Sud, Université Paris-Saclay, F-91406 Orsay, France

E-mail: bakytzhan.urazbekov@gmail.com

Abstract. Angular distributions of protons, deuterons, tritons and alpha particles emitted in the d + ^{9}Be reaction at E_{lab}=19.5 and 35.0 MeV have been measured. The elastic scattering channel is analysed in the framework of both the Optical Model and the Coupled-Channel approach. The interaction potential of the d + ^{9}Be system is calculated in the framework of the Double-Folding model using the $\alpha + \alpha + n$ three-body wave function of the ^{9}Be nucleus. The (d, p) and (d, t) one-nucleon-transfer reactions are analysed within the coupled-reaction-channel approach. The spectroscopic amplitudes for the different nuclear cluster configurations are calculated. Differential cross sections for the reaction channel ^{9}Be$(d, \alpha)^7$Li are calculated including all possible reaction mechanisms within the coupled-reaction-channel method. Corresponding contributions to the cross sections are analysed.

Keywords: cluster structure, optical model, CRC, DWBA, spectroscopic amplitudes, double folding, elastic and inelastic scattering, few-nucleon transfer reactions

1. Introduction

The cluster structure of nuclei arises from a correlated motion of nucleons inside a nucleus. In this regime, a simple subgroup of nucleons can be considered as a single particle. This kind of behaviour can give insights into and better understanding of certain characteristics of the nucleus, as well as affect the processes of nuclear reactions. Investigation of the cluster structure in nuclei is still a priority in modern nuclear physics strongly driven by intensive developments of experimental devices.

There are many stable nuclei in the *p*, *sd* and *pf* shells exhibiting a cluster structure, but ^{9}Be is particularly worthy of attention due to the following reasons:

- a stable nucleus with low binding energies of neutron S_n=1.665 MeV, and α-particle S_α=2.462 MeV [1];
- the deformed shape reflected in the nuclear quadrupole moment, Q= +52.9 mb [2];
- the Borromean structure of the ground state;

These aspects led to take ^{9}Be as a subject for fundamental as well as applied research studies.

Regarding nuclear technologies, ^{9}Be is a good wall material in thermonuclear devices [3, 4]. For instance, for fusion-type devices a value of some dozens of percent of ^{9}Be is expected in the soft wall material [4]. The ^{9}Be nucleus has been chosen as it represents the best compromise based on its characteristic to split by using γ's and e^{-}'s into two energetic α-particles, which are efficient promoters of thermonuclear burning since they can be confined by electromagnetic fields and their energy affects the temperature of the burning zone.

Scattering of the simplest projectiles, such as ^{1,2}H or ^{3,4}He, off a target is a standard tool for fundamental study of the structure of nuclei. This method involves measuring the angular distributions of the nuclear reaction products. It is well known that the energies and angular distributions of projectile-like particles give information about the internal structure of target-like nuclei.

In our previous works [5, 6, 7], the ^{3}He interaction with ^{9}Be was studied and angular distributions of the reaction products in the following exit channels: ^{3}He+^{9}Be, ^{5}He+^{7}Be, ^{5}Li+^{7}Li, ^{6}Be+^{6}He, and ^{6}Li+^{6}Li, were measured. The obtained data were analysed within the framework of the optical-model (OM), the coupled-channel (CC) and the distorted-wave Born approximation (DWBA) approaches. The performed analysis of the experimental data showed sensitivity of the cross sections on the potential parameters in the exit channels. Moreover, these experiments were designed to study the breakup reactions with ^{9}Be in an attempt to determine contributions of the channels with the ^{8}Be+n and ^{5}He+α structure to the inclusive measurements. It was found that these two channels contribute in the ratio of 2.7 to 1, respectively. The determined value justifies that the ^{5}He+α breakup channel plays an important role as well.

Based on the Borromean structure of ^{9}Be, special attention was focused on the breakup processes resulting from the ^{9}Be(^{6}Li, ^{6}Li$'$)^{9}Be* nuclear reaction [8, 9]. The excited nucleus ^{9}Be* can decay either directly into the α+α+n three-body system or through one of the unstable nuclei, such as ^{5}He and ^{8}Be. These relatively recent experimental studies explicitly confirm the cluster structure of ^{9}Be. The calculated branching ratios show that the low-lying excited states, at $E_x < 4.0$ MeV, are mostly populated with the ^{8}Be+n configuration. In other conditions, the ^{5}He+α configuration plays a significant role.

Another aspect of finding the cluster structure is its effect on the nuclear reaction mechanisms. Indeed, since the papers of Detraz *et al.* [10, 11], the multi-particle-multi-hole structures have been expected at rather low excitation energies in nuclei. In such a case, it can be understood that the correlated nucleons are transferred as a whole strongly correlated cluster, which has the internal quantum numbers of a free particle.

The interaction of deuteron and alpha particles with ^{9}Be was studied with regard to the cluster structure [12, 13]. The interaction potential of colliding nuclei was built within the framework of the double-folding model using the three-body wave function. Tests of the double-folded potential were carried out within the OM and DWBA at laboratory energies 10-30 MeV/nucleon. The good agreement obtained in comparison of theoretical cross sections with experimental data led to application of the double-folding potential based on the three-body wave function to study of reactions on ^{9}Be.

The current work is devoted to the investigation of the cluster structure of the ^{9}Be nucleus through studying the nuclear reactions caused by a deuteron

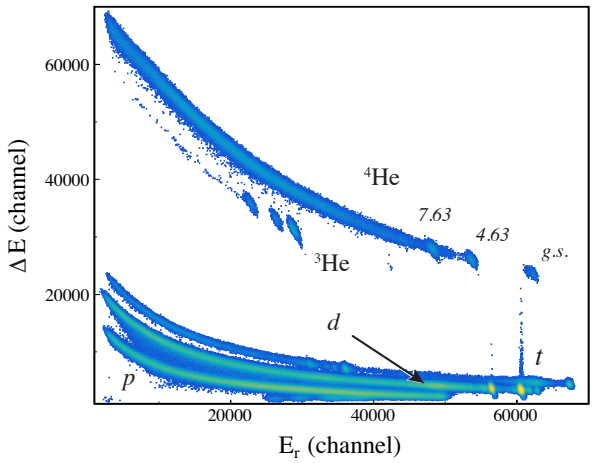

Figure 1. Particle identification plots for the products of the d+^{9}Be reaction at 35 MeV incident energy: p, d, t, and ^{3,4}He. ΔE is the energy loss and E$_r$ is the residual energy. ^{7}Li excited states in the ^{7}Li reaction channel, i.e. ^{7}Li+α, are indicated.

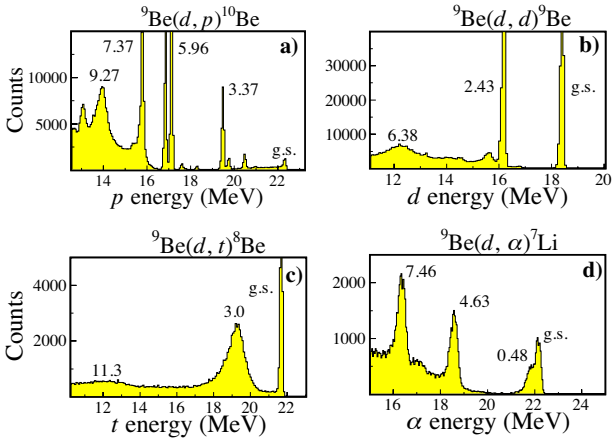

Figure 2. Spectra of total deposited energy measured at θ_{lab}=32° for the detected p (panel a), d (panel b), t (panel c), and α (panel d). The ground and the excited states of ^{7}Li for the detected complementary product α as well as the ground states and the excited states for ^{8}Be, ^{9}Be, and ^{10}Be in the case of detected t, d, and p, as complementary products, respectively, are unambiguously identified.

beam at 19 MeV and 35 MeV incident energies. In the exit channel, the simplest particles, such as p, d, t, and α-particles, were registered and their angular distributions were obtained. A comparative analysis of experimental data and theoretical calculations has been performed.

2. Experimental Method

The experiment has been performed at the INP (Řež, Czech Republic) and at the Physics Department of Jyväskylä University (Jyväskylä, Finland). The beam energy of ^{2}H ions produced from the cyclotrons were at energies 19.5 and 35 MeV. The average beam current during the experiment was maintained at 20 nA. The self-supporting ^{9}Be target was prepared from a thin beryllium foil with 99 % purity. A set of four telescopes was used for registering particles from output channels. Each telescope comprised ΔE$_0$, ΔE, E$_r$ detectors with the respective thicknesses of 12 μm, 100 μm and 3 mm. To detect reaction products with well-defined good angular resolution, telescopes were mounted at a distance of ∼25 cm from the target. Each telescope was shielded by a Cu-Pb collimator with a thickness of 3 mm and hole with a diameter of 3 mm. The telescopes were mounted on rotating supports, which allow us to obtain data from $\theta_{lab} = 20°$ to 107° in steps of $1 - 2°$.

The particles were identified based on the energy-loss measurements of ΔE and the residual energy E$_r$, i.e., by the so-called ΔE-E method. An example of two-dimensional plots (yield vs. energy loss ΔE and residual energy E$_r$) is shown in Fig. 1.

Current experimental technique allow identification of the particles p, d, t, and α and determination of their total deposited energies. The spectra of total deposited energies are shown in Fig. 2. All the peaks in Fig. 2 have been identified and assigned to the ground and excited states of ^{10}Be, ^{9}Be, ^{8}Be, and ^{7}Li nuclei as the complementary products for the detected particles p, d, t, α, respectively.

3. Data Analysis and Results

3.1. Elastic scattering

The theoretical calculations of the deuteron elastic scattering on ^{9}Be at 19.5 and 35 MeV energies have been performed in the framework of the OM with the OM potential given by:

$$U(R) = -V^V(R) - iW^V(R) + V^{SO}(R)(\mathbf{l}\cdot\sigma) + V^C(R), \quad (1)$$

where V^V, W^V, V^{SO}, and V^C are real volume, imaginary volume, spin-orbit and Coulomb potentials, respectively. In this work, the real part of the OM potential was obtained by means of the double-folding (DF) model

$$V^V(R) = N_R V^{DF}(R) \quad (2)$$

with normalization factor N_R. For convenience, in the OM and CC (CRC) calculations the potential can be fitted by means of the sum of three Woods-Saxon potentials:

$$V^V(R) = \sum_{i=1}^{3} V^i f^{R_i,a_i}(R), \quad (3)$$

$$f^{R_V,a_V}(R) = \frac{1}{1 + exp\frac{R-R_V}{a_V}}. \quad (4)$$

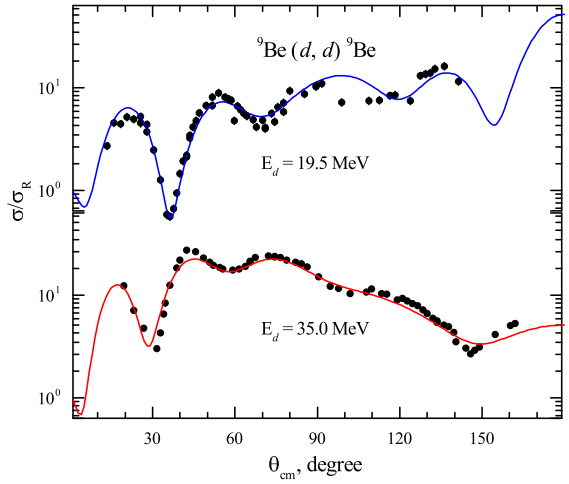

Figure 3. The angular distribution of elastic scattering data of d from ^{9}Be at laboratory energy 19.5 MeV in comparison with theoretical calculations within the OM (solid curve).

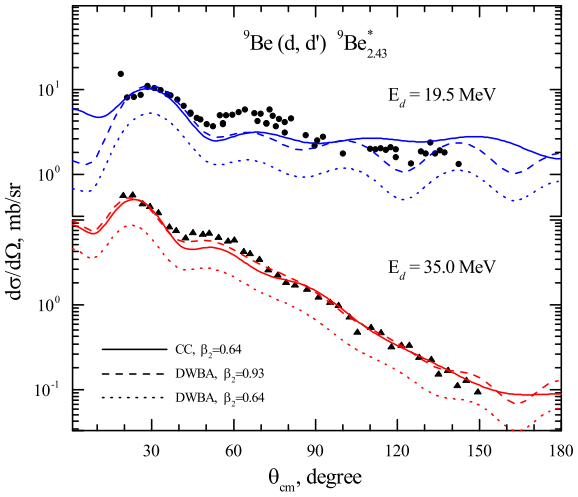

Figure 4. The cross sections of inelastic scattering ^{9}Be$(d,d)^9$Be* (E$_{exc}$=2.43 MeV) at laboratory energies 19.5 MeV (full circle) and 35 MeV (full triangle). Theoretical curves are described in the text.

The DF potential was calculated using the effective M3Y-Paris nucleon-nucleon potential and the nuclear-matter-densities of projectile and target nuclei. In order to calculate the ^{9}Be matter distribution we applied the $\alpha + \alpha + n$ three-body model (for more details, see Ref. [12]), while the matter density distribution of the deuteron projectile was chosen to be of the form

$$\rho\left(\frac{1}{2}r\right) = \int |\Psi(\mathbf{r})|^2 d\Omega_r. \quad (5)$$

The spin-orbit term of the OM potential has standard form

$$V^{SO}(R) = V_0^{SO}\left(\frac{\hbar}{m_\pi c}\right)^2 \frac{1}{R}\frac{d}{dR} f^{R_{SO}a_{SO}}(R). \quad (6)$$

The Coulomb term has been taken as the interaction of a point-charge with a uniformly charged sphere

$$V^C(R) = \begin{cases} \dfrac{Z_1 Z_2 e^2}{2R_C}\left(3 - \dfrac{R^2}{R_C^2}\right), & \text{for R} \le R_C, \\ \dfrac{Z_1 Z_2 e^2}{R}, & \text{for R} > R_C\ . \end{cases} \quad (7)$$

The parameters of the imaginary part of the optical potential were obtained by fitting the theoretical cross sections to the experimental data at 19.5 MeV and 35 MeV incident energies. As a starting point, the same parameterizations of the real part were used. The obtained potential parameters after fitting are listed in Table 1 for both 19.5 MeV and 35.0 MeV incident energies.

The comparison of the results of the theoretical calculations with the measured data for elastic scattering at 19.5 MeV and 35.0 MeV energies are plotted in Fig. 3. The cross sections obtained in the framework of the OM with the DF potential are shown as solid curves. Theoretical results obtained by means of the OM give an excellent agreement, $\chi^2 \approx 2.5$, with the experimental data. The parameters of parameterized double-folding potential are listed in Table 1.

Table 1. Parameterized double-folding potentials of the d+^{9}Be system used in the OM, CC and DWBA calculations.

E$_d$, MeV	i	V$_0$, MeV	r^a_v, fm	a$_v$, fm	W$_0$, MeV	r^a_w, fm	a$_w$, fm	V$_0^{SO}$, MeV	N$_R$,	r^a_C, fm	χ^2/N
19.5	1	6.18	0.328	0.308	3.99	0.328	0.127	3.275	1.22	0.809	2.490
	2	70.97	0.746	0.831	25.50 (17.5^b)	0.746	0.766				
	3	0.605	1.491	1.724	0.924	1.491	2.238				
35.0	1	5.941	0.328	0.308	7.07	0.612	0.108	3.275	1.17	0.809	2.503
	2	68.68	0.746	0.831	22.50 (17.5^b)	0.838	0.731				
	3	0.58	1.491	1.724	0.999	1.377	1.856				

[a] Radii are defined as $R_i = r_i\left(A_P^{1/3} + A_T^{1/3}\right)$.

[b] The values are used in CRC calculations.

3.2. Inelastic scattering

The CC and DWBA approaches have been applied to analyse the measured inelastic scattering data corresponding to the ^{9}Be($5/2^-$, 2.43 MeV) excitation. Calculations were performed employing the FRESCO code [14] and the DWUCK5 code [15] which are available in the NRV knowledge-base [16].

In order to describe the measured experimental data one has to consider the ^{9}Be target having a quadrupole deformation. Thus, the ^{9}Be spectrum consists of the rotational band including the $3/2^-$ ground state, $5/2^-$ state at 2.43 MeV and $7/2^-$ state at 6.38 MeV. Couplings to these states were taken into account within the coupled-channel approach. The spin reorientations were also taken into account. The coupling interaction has the usual form:

$$V_\lambda(R) = -\beta_\lambda R_V \left|\frac{dV^V}{dR}\right| - i\beta_\lambda R_W \left|\frac{dW^D}{dR}\right|, \qquad (8)$$

where β_λ is the deformation parameter of λ multipole describing the target-nucleus form. Here, we neglect as usual the contribution of the Coulomb interaction.

The calculated cross sections for inelastic scattering to the $5/2^-$ state at 2.43 MeV are shown in Fig. 4. The solid curves correspond to the results obtained within the CC approach, while the dashed and dotted curves were obtained within the DWBA approach using different values of the deformation parameter β_2. The used potential parameters are listed in Table 1.

All the results in Fig. 4 are in good agreement with the experimental data, except for the cross sections around 60° at 19.5 MeV incident energy. The quadrupole deformation parameter $\beta_2 = 0.64$ extracted within the coupled-channel model is consistent with the previous studies [5, 17].

In the case of DWBA calculations, one uses the DF potential (see Table 1) for both the entrance and the exit channels. The DWBA angular distributions very well reproduce the structure of experimental data but clearly underestimate them when the deformation parameter $\beta_2 = 0.64$ is used (see the dotted curves in Fig. 4). In order to get the best fit the deformation parameter must be increased up to $\beta_2 = 0.93$, which is quite close to the values reported in previous studies (see, for example, [18, 19]).

Thus, one may confirm that channel coupling and the effects of spin reorientation enhance the cross section that results in the reduction of the deformation parameter. However, the DWBA approach takes into account only first-order contributions to the transition amplitude. In particular, it also describes only general features of the angular distributions and overestimates the deformation parameter in order to compensate the difference between the experimental data and the DWBA cross sections.

3.3. One-nucleon transfer reactions

The one-neutron pick-up ^{9}Be$(d,t)^8$Be and stripping ^{9}Be$(d,p)^{10}$Be reactions were analyzed here within the framework of the Coupled Reaction Channels (CRC).

The double-folding potential given in Table 1 was used in the CRC calculations for the entrance channel and the global optical parameterizations from Ref. [20, 21] were used for the exit channels. The coupling schemes of target and daughter nuclei for the ^{9}Be$(d,p)^{10}$Be and ^{9}Be$(d,t)^8$Be reactions are illustrated in Fig. 5. The states of ^{10}Be, 2^+_1 and 2^+_2, as well as the low-lying excited states of ^{8}Be, 2^+ and 4^+, were included in the coupling scheme. Also, the schemes take into account the spin reorientations of states on the condition $J \neq 0$.

In order to construct the bound-state wave functions of the transferred particle in the entrance and exit channels, the common method, i.e. fitting the depth of the corresponding Woods-Saxon potential to the known binding energy, was employed. The reduced radius and diffuseness in this case are set to be $r = 1.25$ fm and $a = 0.65$ fm, respectively. If the transfer takes place to a final unbound state, the depth of the potential for this state was adjusted to yield a binding energy equal to -0.1 MeV in accordance with the procedure used in Ref. [17].

The spectroscopic amplitude $\mathcal{S}$ for the addition of a particle to a core with angular momentum J_{core} to form a composite with J_{com} is related to the matrix element of the creation operator $\hat{a}^\dagger$:

$$\mathcal{S}_{Nlj} = \frac{\langle J_{com} \| \hat{a}^\dagger_{Nlj} \| J_{core} \rangle}{\sqrt{2J_{com}+1}} \qquad (9)$$

where Nlj is the set of particle quantum numbers. The spectroscopic amplitudes for one particle states

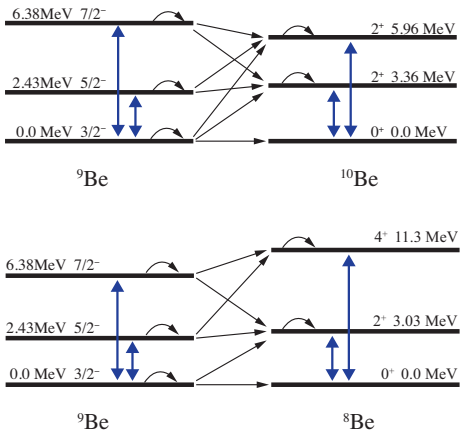

Figure 5. The target coupling schemes in the ^{9}Be$(d,p)^{10}$Be (upper) and the ^{9}Be$(d,t)^8$Be (lower) nuclear reactions. The bold two-headed arrows indicate Eλ transitions. The spin reorientation effects are indicated as back-pointing arrows.

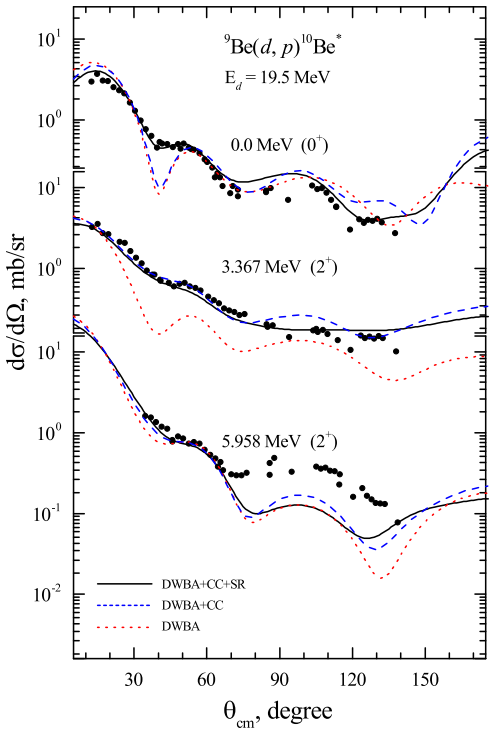

Figure 6. Differential cross sections for the ^{9}Be$(d,p)^{10}$Be* reactions at 19.5 MeV leading to different final states (labelled in the figure) in ^{10}Be. The experimental data are shown in comparison with theoretical results obtained within the CRC method.

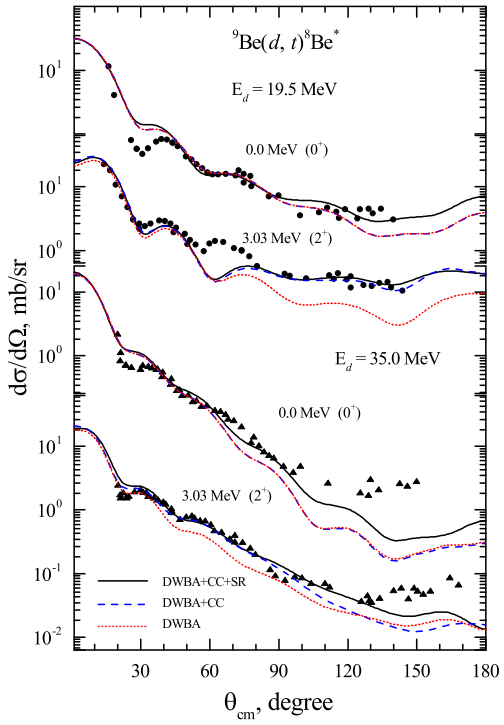

Figure 7. Differential cross sections for the ^{9}Be$(d,t)^8$Be* reactions at 19.5 and 35 MeV leading to different final states (labelled in the figure) in ^{8}Be. The experimental data are shown in comparison with theoretical results obtained within the CRC method.

were calculated by means of the *ANTOINE* code [22] using the effective Cohen-Kurath interaction for p-shell nuclei [23]. The calculated spectroscopic amplitudes for the one-nucleon transfer reactions are listed in Table 2.

Angular distributions of the ^{9}Be$(d,p)^{10}$Be nuclear reaction at E$_d$=19.5 MeV are shown in comparison with the theoretical curves calculated in the framework of the CRC method in Fig. 6.

In order to study the couplings of the input channels, the outputs were fixed using the deformation parameter of ^{8}Be from Ref. [26], and for ^{10}Be from Ref. [17]. The direct transition from the ground state is indicated by the dotted line (DWBA). The contributions of the transitions from excited states (CC), and from spin reorientations (SR) are indicated by dashed and solid lines, respectively. During the analysis, it was found that spin reorientation has a significant contribution in the p + ^{10}Be$_{gs}$ channel, especially in the range of 40-60 degrees. It is interesting to note that we managed to describe within the CRC method the differential cross section of the ^{9}Be$(d,p)^{10}$Be$_{gs}$ reaction at all scattering angles, including the range 40°-60°, where they were not covered in Refs. [27, 18].

An appreciable contribution of the $3/2^- \rightarrow 2^+_1$, $5/2^- \rightarrow 2^+_1$, $7/2^- \rightarrow 2^+_1$ transitions was observed in the p + ^{10}Be$_{3.37}$ channel in the entire range of scattering angles. In the cross section of the p + ^{10}Be$_{5.96}$ channel, the theoretical calculation underestimates the experimental data starting from 70°. Possibly, other higher excited states of ^{9}Be should be taken into account.

Figure 7 displays the cross sections of the ^{9}Be$(d,t)^8$Be nuclear reaction at both 19.5 MeV and 35 MeV incident energies. As in the case of the (d,p) reactions, the (d,t) reactions also show the strong channel-coupling effects. We see a manifestation of spin-reorientation effects in the t+^{8}Be$_{gs}$ channels and a significant contribution of the $3/2^- \rightarrow 2^+$, $5/2^- \rightarrow 2^+$, $7/2^- \rightarrow 2^+$ transitions in the t+^{8}Be$_{3.03}$ channel. Disagreements around 30° in the t+^{8}Be$_{gs}$ channel for both 19.5 MeV and 35 MeV incident energies and around 60° in the t+^{8}Be$_{3.03}$ channel for 19.5 MeV incident energy are possibly caused by the uncertainty in the t+^{8}Be interaction potential.

Theoretical calculations made within the CRC method show, in general, good agreement with the experimental data for both (d,p) and (d,t) reactions. The analysis showed strong coupling effects in both entrance and exit channels. The effects of such couplings were also emphasized in Refs. [17, 28].

Table 2. Spectroscopic amplitudes used in CRC calculations for the Composite = Core + Cluster system. The one-nucleon spectroscopic amplitudes have been calculated by means of the *ANTOINE* code [22]. The alpha spectroscopic amplitudes were taken from [24, 25].

Composite	$2J_{com}$	Core	$2J_{core}$	Cluster	2J	SA	Composite	$2J_{com}$	Core	$2J_{core}$	Cluster	2J	SA
^{9}Be	3	^{8}Be	0	n	3	−0.761	^{9}Be	3	^{8}Li	2_1	p	1	−0.444
^{9}Be	3	^{8}Be	4	n	3	0.816	^{9}Be	3	^{8}Li	6	p	3	−0.592
^{9}Be	3	^{8}Be	4	n	1	−0.242	^{9}Be	3	^{8}Li	2_2	p	3	−0.236
^{9}Be	5	^{8}Be	4	n	3	0.986	^{9}Be	3	^{8}Li	2_2	p	1	0.036
^{9}Be	5	^{8}Be	4	n	1	−0.417	^{9}Be	5	^{8}Li	4	p	3	0.593
^{9}Be	5	^{8}Be	8	n	3	−0.374	^{9}Be	5	^{8}Li	4	p	1	0.515
^{9}Be	7	^{8}Be	4	n	3	−0.457	^{9}Be	5	^{8}Li	2_1	p	3	−0.672
^{9}Be	7	^{8}Be	8	n	3	0.919	^{9}Be	5	^{8}Li	6	p	3	−0.571
^{9}Be	7	^{8}Be	8	n	1	−0.429	^{9}Be	5	^{8}Li	6	p	1	−0.171
^{8}Be	0	^{7}Li	3	p	3	−1.204	^{9}Be	5	^{8}Li	2_2	p	3	0.200
^{8}Be	0	^{7}Li	1	p	1	0.736	^{9}Be	7	^{8}Li	4	p	3	−0.323
^{8}Be	4	^{7}Li	3	p	3	−0.748	^{9}Be	7	^{8}Li	6	p	3	−0.899
^{8}Be	4	^{7}Li	3	p	1	−0.612	^{9}Be	7	^{8}Li	6	p	1	−0.564
^{8}Be	4	^{7}Li	1	p	3	0.667	^{7}Li	3	^{6}Li	2	n	3	0.657
^{8}Be	4	^{7}Li	7	p	3	0.624	^{7}Li	3	^{6}Li	2	n	1	−0.538
^{8}Be	4	^{7}Li	5_2	p	3	0.079	^{7}Li	3	^{6}Li	6	n	3	0.744
^{8}Be	4	^{7}Li	5_2	p	3	−0.146	^{7}Li	3	^{6}Li	4	n	3	−0.032
^{8}Be	8	^{7}Li	7	p	3	0.864	^{7}Li	3	^{6}Li	4	n	1	0.399
^{8}Be	8	^{7}Li	7	p	1	0.687	^{7}Li	1	^{6}Li	2	n	3	−0.925
^{8}Be	8	^{7}Li	5_2	p	3	0.374	^{7}Li	1	^{6}Li	2	n	1	0.197
^{8}Li	4	^{7}Li	3	n	3	−0.988	^{7}Li	1	^{6}Li	4	n	3	−0.555
^{8}Li	4	^{7}Li	3	n	1	0.237	^{7}Li	7	^{6}Li	6	n	3	−0.936
^{8}Li	4	^{7}Li	1	n	3	0.430	^{7}Li	7	^{6}Li	6	n	1	0.645
^{8}Li	4	^{7}Li	7	n	3	−0.496	^{7}Li	7	^{6}Li	4	n	3	−0.456
^{8}Li	4	^{7}Li	5	n	3	−0.665	^{7}Li	5_2	^{6}Li	2	n	3	−0.650
^{8}Li	4	^{7}Li	5_2	n	1	−0.275	^{7}Li	5_2	^{6}Li	6	n	3	0.732
^{8}Li	2_1	^{7}Li	3	n	3	0.567	^{7}Li	5_2	^{6}Li	6	n	1	0.549
^{8}Li	2_1	^{7}Li	3	n	1	0.351	^{7}Li	5_2	^{6}Li	4	n	3	0.200
^{8}Li	2_1	^{7}Li	1	n	3	0.905	^{7}Li	5_2	^{6}Li	4	n	1	−0.114
^{8}Li	2_1	^{7}Li	1	n	1	0.331	^{6}Li	2	d	2	α	0	0.907
^{8}Li	2_1	^{7}Li	5_2	n	3	0.767	^{6}Li	2	d	2	α	4	0.077
^{8}Li	6	^{7}Li	3	n	3	0.581	^{6}Li	6	d	2	α	4	0.943
^{8}Li	6	^{7}Li	5_2	n	3	−0.660	^{6}Li	6	d	2	α	8	0.028
^{8}Li	6	^{7}Li	5_2	n	1	−0.541	^{6}Li	4	d	2	α	4	0.929
^{8}Li	6	^{7}Li	7	n	3	0.973	^{9}Be	3	^{5}He	3	α	0	−0.925
^{8}Li	6	^{7}Li	7	n	1	−0.404	^{9}Be	3	^{5}He	3	α	4	0.784
^{8}Li	2_2	^{7}Li	3	n	3	−0.617	^{9}Be	5	^{5}He	3	α	4	0.974
^{8}Li	2_2	^{7}Li	3	n	1	−0.841	^{9}Be	5	^{5}He	3	α	8	−0.260
^{8}Li	2_2	^{7}Li	1	n	3	0.178	^{9}Be	7	^{5}He	3	α	4	0.882
^{8}Li	2_2	^{7}Li	1	n	1	0.331	^{9}Be	7	^{5}He	3	α	8	−0.737
^{8}Li	2_2	^{7}Li	5	n	3	0.231	^{7}Li	3	t	1	α	1	0.970
^{9}Be	3	^{8}Li	4	p	3	−0.947	^{7}Li	1	t	1	α	1	0.961
^{9}Be	3	^{8}Li	4	p	1	−0.319	^{7}Li	7	t	1	α	3	0.952
^{9}Be	3	^{8}Li	2_1	p	3	0.454	^{7}Li	5_2	t	1	α	3	0.223

3.4. Cluster-transfer reaction

Differential cross sections for the nuclear reaction ^{9}Be$(d,\alpha)^{7}$Li are of particular interest. This is due to the specific behaviour of the cross section at large scattering angles, which indicates a ^{5}He cluster transfer. In addition, the cross section calculated within the DWBA approach underestimates the data even at forward scattering angles. Therefore, in order to understand the difference between theory and experiment, the following transfer mechanisms are suggested (see Fig. 9):

– direct transfer of heavy clusters d and ^{5}He;

– sequential two-step transfer of n-p, p-n, n-α and α-n;

The resulting differential cross section for the ^{9}Be$(d,\alpha)^{7}$Li reaction has the form of a coherent sum of two amplitudes

$$\frac{d\sigma}{d\Omega}(\theta) = |f_I(\theta) + f_{II}(\theta)|^2, \quad (10)$$

where the amplitude

$$f_I(\theta) = f_{^5\mathrm{He}}(\pi-\theta) + f_{n\text{-}\alpha}(\pi-\theta) + f_{\alpha\text{-}n}(\pi-\theta) \quad (11)$$

describes the transfer of the heavy ^{5}He-cluster and sequential two-step transfer of n-α and α-n, and the

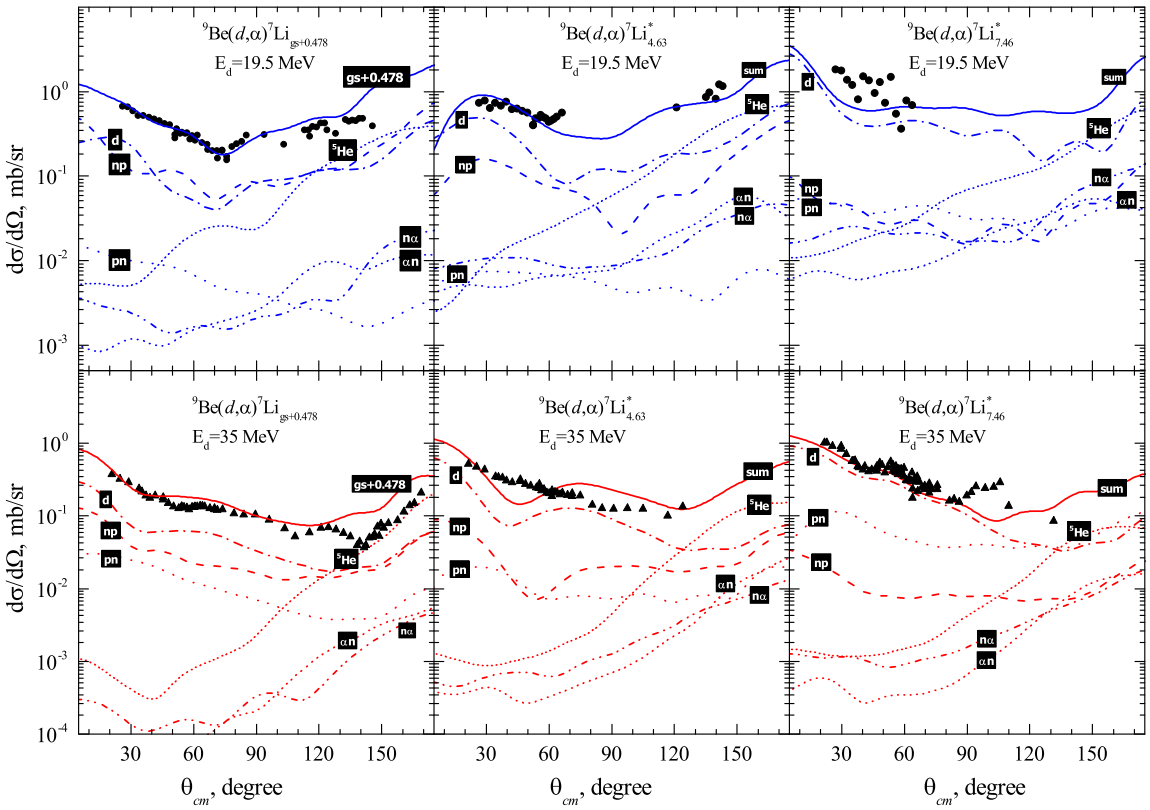

Figure 8. Differential cross sections for the ^{9}Be(d,α)^{7}Li reactions measured at 19.5 MeV and 35 MeV energy with the ^{7}Li observed in the ground or low-lying excited states in the exit channels.

amplitude

$$f_{II}(\theta) = f_d(\theta) + f_{n\text{-}p}(\theta) + f_{p\text{-}n}(\theta) \qquad (12)$$

corresponds to the deuteron pick-up and sequential two-step transfer of n-p and p-n.

The DF potential (see Table 1) for the entrance channel and global optical potential parameterizations from Refs. [21, 29, 30] for intermediate and exit channels were used in the analysis. The prior form for the first coupling and the post form for the second coupling were chosen for two-step transfer reactions in order to avoid the non-orthogonal terms in the calculations of transition amplitudes.

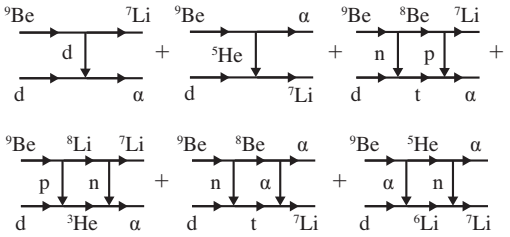

Figure 9. The scheme illustrates the reaction mechanisms taken into account in CRC calculations of the cross sections for ^{9}Be(d, α)^{7}Li reaction.

The spectroscopic amplitudes of the d and ^{5}He clusters were taken from Ref. [31], while the alpha-cluster spectroscopic amplitudes given in Table 2 were provided by Dr. A. Volya within the method reported in Ref. [25].

The calculated cross sections are shown in Fig. 8 with the α-particle angular distributions formed in the ^{9}Be(d,α)^{7}Li* reaction at incident energies of 19.5 and 35 MeV and corresponding to the low-lying excitation of the ^{7}Li nucleus in the exit channels. The transfer of the deuteron (dash-dotted curve) provides the dominant contribution in all the channels. Despite the fact that the spectroscopic amplitude of the deuteron $\mathcal{S}_{1D_3} = 0.558$ in the ^{9}Be nucleus is not of great importance, a noticeable cross section is due to the large value of the deuteron spectroscopic amplitude $\mathcal{S}_{1S_1} = 1.732$ of ^{4}He.

The angular distribution of deuteron transfer has a significant cross section also at the backward scattering angles, which is mainly caused by the contribution of the D wave. This symmetrical behaviour of the cross section of D waves is very similar to the cross section of evaporation residues. Tanaka *et al.* [32] analyzed the role of the compound process in ^{9}Be(d, α)^{7}Li reaction and claimed the domination of the compound nucleus

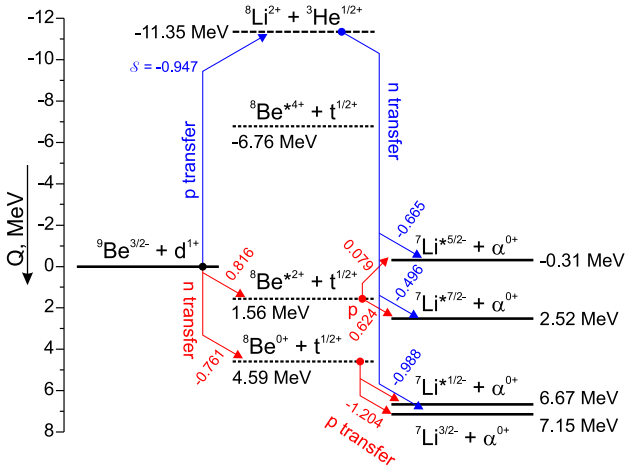

Figure 10. The scheme illustrates the energy balance of the different intermediate stages for the two-step mechanisms of ^{9}Be$(d,\alpha)^{7}$Li transfer reaction. The Q-values for the different intermediate channels are shown near the corresponding lines. The numbers near the arrows correspond to the spectroscopic amplitudes of the heaviest reaction participants. For example, spectroscopic amplitude for the $^{9}\text{Be} = {}^{8}\text{Li} + p$ configuration is equal $\mathcal{S} = -0.947$.

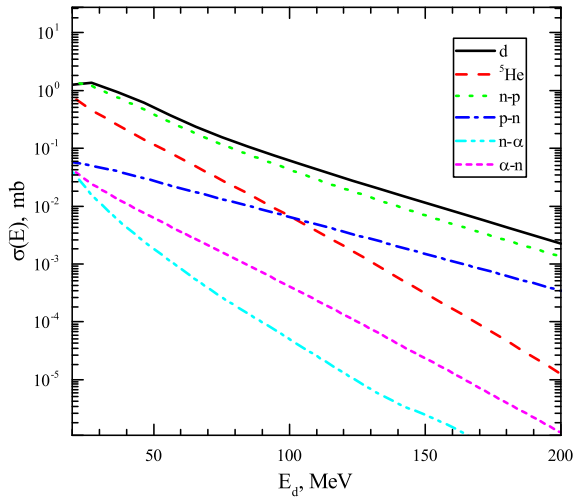

Figure 11. Contributions of the different mechanisms to the cross section of the ^{9}Be$(d,\alpha)^{7}$Li$_{g.s.}$ reaction. See Fig. 9 for explanation of the curve notations.

channels at the energies of 12.17 MeV and 14.43 MeV. However, in Ref. [18] the negligible contribution of the compound-nucleus mechanism was shown at 7 MeV using the DWBA analysis. In this regard, our theoretical results based on the CRC method show that there is no need to take into account the mechanism through the compound-nucleus formation at energies of 19.5 and 35.0 MeV.

Starting from scattering angle $\theta_{c.m.} = 120°$, the transfer of the ^{5}He cluster, labeled as ^{5}He in Fig. 8, has a predominant contribution in all channels. It should be noted that a similar result was reported earlier in Ref. [18]. One-step transfer of the ^{5}He cluster was also indicated as a dominant process by Jarczyk *et al.* [33] in studying the ^{12}C(^{11}B,^{6}Li)^{17}O and ^{12}C(d,^{7}Li)^{7}Be reactions.

Using the CRC method, we are able to estimate the contribution of the sequential transfer of ^{5}He, which was not studied before. Corresponding cross sections are shown in Fig. 8 as curves labeled $n\alpha$ and αn. It turned out that the n-α and α-n transfer processes provide indeed a contribution more than one order of magnitude smaller in comparison with the one-step ^{5}He transfer. Nevertheless, it should be noted that the contribution of the n-α and the α-n transfer channels increases with the increase in the ^{7}Li excitation energy, where they should not be ignored.

The two-step n-p transfer is another mechanism providing a noticeable contribution to the cross section. It is due to the prominent cluster structure of the ^{9}Be nucleus having the weakly bound neutron. This structural feature explains also the weakness of the p-n sequential transfer contribution to the cross section corresponding to the ^{7}Li(g.s.) in the exit channel. However, with increasing the ^{7}Li excitation energy these two mechanisms are interchanged in the significance of their contributions, as depicted by the curves in Fig. 8, and the p-n transfer begins to play a leading role, providing, in particular, almost 10 times larger contribution in the case of reaction at $E_{lab} = 35$ MeV with ^{7}Li*(7.46 MeV) in exit channel.

In Fig. 10, the possible scenarios for the n-p and p-n sequential transfer for the reaction under consideration are shown in respect to the Q-values. One may see that all the steps of the n-p sequential transfer have positive Q-values, while the p-n transfer goes through the intermediate channel ^{8}Li + ^{3}He that has a considerably negative Q-value. Together with the large values of the spectroscopic amplitudes (shown near to the arrows in Fig. 10), this explains the leading role of the $(d,t;t,\alpha)$ mechanism in populating the ground state of ^{7}Li in the exit channel.

The situation becomes quite different in the case of the ^{7}Li$^{*}(5/2^{-})$ in the exit channel. First, the population of this state through the n-p transfer involves the $^{9}\text{Be} = {}^{8}\text{Be}^{*}(2^{+}) + n$ intermediate configuration where the ^{8}Be cluster has to be in the 2^{+} excited state. Note that the ^{8}Be(0^{+}) ground state is inappropriate because of angular-momentum-coupling mismatch in the entrance and exit configurations. Second, the extremely small spectroscopic amplitude of the $^{8}\text{Be}^{*}(2^{+}) = {}^{7}\text{Li}^{*}(5/2^{-}) + p$ configuration, which is $\mathcal{S} = 0.079$, influences the transfer amplitude. These two factors lead to the suppression of the contribution of $(d,t;t,\alpha)$ mechanism in population of the ^{7}Li$^{*}(5/2^{-})$ state in the exit channel. Therefore, the p-n sequential transfer prevails over the n-p one.

Figure 11 shows the contributions of all the mechanisms mentioned above to the total cross section of the ^{9}Be$(d,\alpha)^7$Li$_{g.s.}$ reaction (see Fig. 9) as a function of the deuteron energy. One may conclude that mainly four mechanisms contribute to the cross section of this reaction. The transfer of the deuteron-cluster is the predominant channel at all collision energies. The sequential *n*-*p* and *p*-*n* transfers play a significant role at the high energies. The ^{5}He-cluster transfer gives almost 20% of the cross section at low energies and outdoes the sequential *p*-*n* transfer in this energy domain. This allows us to claim that the configurations n+^{8}Be and $\alpha + {}^5$He provide noticeable contributions to the ground-state wave function of the ^{9}Be nucleus. These conclusions agree well with the previous experimental studies [8, 9].

4. Conclusion

In the present work, the deuteron-induced reactions on a ^{9}Be target have been studied at the collision energies 19.5 and 35 MeV. The calculated double-folding potential has been applied successfully in describing the cross sections of elastic and inelastic scatterings, one-nucleon transfer and cluster-transfer reactions. The deformation parameter for the transition $3/2^- \rightarrow 5/2^-$ of ^{9}Be has been determined. The strong coupling effects have been shown for the (d,p) and (d,t) one-nucleon transfer nuclear reactions. Furthermore, it was found that in the ^{9}Be$(d,\alpha)^7$Li nuclear reaction the ^{5}He heavy cluster is transferred mainly simultaneously, and the contribution of its sequential transfer is an order of magnitude lower. The importance of taking into account the mechanism of sequential transfer of the *n*-*p* system has been revealed. Based on these observations from studying the interaction of the deuteron with ^{9}Be, it can be concluded that the ^{9}Be nucleus has cluster structure.

Acknowledgments

The authors acknowledge the support of the CANAM project [34] for providing beam time for the experiment. The authors are also grateful to I. Thompson for advising on the FRESCO code and to A. Volya for providing the alpha spectroscopic amplitudes. V.K, V.B and J.M. acknowledge the support of the MEYS project EF16-013/0001679.

This work was supported by the Russian Science Foundation (17-12-01170).

References

[1] Wang M, Audi G, Wapstra A H, Kondev F G, MacCormick M, Xu X and Pfeiffer B 2012 *Chin. Phys. C* **36** 1603
[2] Sundholm D and Olsen J 1991 *Chem. Phys. Lett.* **177** 91
[3] Kukulin V I and Voronchev V T 2010 *Phys. At. Nucl.* **73** 1376
[4] Seksembayev Z, Kukulin V and Sakhiyev S 2018 *Phys. Scr.* **93** 085602
[5] Lukyanov S M, Denikin A S, Voskoboynik E I, Khlebnikov S V, Harakeh M N, Maslov V A, Penionzhkevich Y E, Sobolev Y G, Trzaska W H, Tyurin G P and Kuterbekov K A 2014 *J. Phys. (London)* **G41** 035102
[6] Lukyanov S M, Harakeh M N, Naumenko M A, Xu Y, Trzaska W H, Burjan V, Kroha V, Mrazek J, Glagolev V, Piskor S, Voskoboynik E I, Khlebnikov S V, Penionzhkevich Y E, Skobelev N K, Sobolev Y G, Tyurin G P, Kuterbekov K and Tuleushev Y 2015 *World Journal of Nuclear Science and Technology* **5** 265
[7] Janseitov D M, Lukyanov S M, Mendibayev K, Penionzhkevich Y E, Skobelev N K, Sobolev Y G, Kuterbekov K A, Valiolda D S, Zholdybayev T K, Trzaska W H, Khlebnikov S V, Tyurin G P, Urazbekov B A, Harakeh M N, Burjan V, Kroha V, Mrazek J, Piskor S, Sivacek I and Glagolev V 2018 *Int. J. Mod. Phys.* **E27** 1850089
[8] Brown T A D, Papka P, Fulton B R, Watson D L, Fox S P, Groombridge D, Freer M, Clarke N M, Ashwood N I, Curtis N, Ziman V, McEwan P, Ahmed S, Catford W N, Mahboub D, Timis C N, Baldwin T D and Weisser D C 2007 *Phys. Rev.* **C76** 054605
[9] Papka P, Brown T A D, Fulton B R, Watson D L, Fox S P, Groombridge D, Freer M, Clarke N M, Ashwood N I, Curtis N, Ziman V, McEwan P, Ahmed S, Catford W N, Mahboub D, Timis C N, Baldwin T D and Weisser D C 2007 *Phys. Rev.* **C75** 045803
[10] Detraz C, Duhm H H and Hafner H 1970 *Nucl. Phys.* **A147** 488
[11] Detraz C, Pougheon F, Bernas M, Langevin M, Roussel P and Vernotte J 1974 *Nucl. Phys.* **A228** 39
[12] Urazbekov B A, Denikin A S, Sakhiev S K and Burtebaev N T 2016 *Bull. Rus. Acad. Sci. Phys.* **80** 247
[13] Urazbekov B A, Denikin A S, Sakhiev S K and Lukyanov S M 2017 *Bull. Rus. Acad. Sci. Phys.* **81** 690
[14] Thompson I J 1988 *Comp. Phys. Rep.* **7** 167 – 212
[15] Kunz P D Computer code DWUCK5 unpublished
[16] Karpov A, Denikin A, Naumenko M, Alekseev A, Rachkov V, Samarin V, Saiko V and Zagrebaev V 2017 *Nucl. Instr. and Meth. Phys. Res.t* **A859** 112 – 124
[17] Harakeh M N, van Popta J, Saha A and Siemssen R H 1980 *Nucl. Phys.* **A344** 15
[18] Szczurek A, Bodek K, Krug J, Lubcke W, Ruhl H, Steinke M, Stephan M, Kamke D, Hajdas W, Jarczyk L, Kamys B, Strzalkowski A and Kwasniewicz E 1989 *Z. Phys.* **A333** 271
[19] Votava H J, Clegg T B, Ludwig E J and Thompson W J 1973 *Nucl. Phys.* **A204** 529
[20] Koning A J and Delaroche J P 2003 *Nucl. Phys.* **A713** 231
[21] Li X, Liang C and Cai C 2007 *Nucl. Phys.* **A789** 103
[22] Caurier E, Martínez-Pinedo G, Nowacki F, Poves A and Zuker A P 2005 *Rev. Mod. Phys.* **77**(2) 427–488
[23] Cohen S and Kurath D 1965 *Nucl. Phys.* **73** 1
[24] Volya A *Private communication. Unpublished*
[25] Kravvaris K and Volya A 2017 *Phys. Rev. Lett.* **119** 062501
[26] Della Rocca V and Iachello F 2018 *Nucl. Phys.* **A973** 1
[27] Galanina L I and Zelenskaya N S 2012 *Phys. Part. Nucl.* **43** 147
[28] Rudchik A T, Chercas K A, Kemper K W, Rusek K, Rudchik A A, Herashchenko O V, Koshchy E I, Pirnak V M, Piasecki E, Trzcinska A, Sakuta S B, Siudak R, Strojek I, Stolarz A, Ilyin A P, Ponkratenko O A, Stepanenko Y M, Shyrma Y O, Szczurek A and Uleshchenko V V 2016 *Nucl. Phys.* **A947** 161
[29] Avrigeanu V, Hodgson P E and Avrigeanu M 1994 *Phys. Rev.* **C49** 2136
[30] Cook J 1982 *Nucl. Phys.* **A388** 153

[31] Kwasniewicz E and Jarczyk L 1985 *Nucl. Phys.* **A441** 77
[32] Tanaka S 1978 *J. Phys. Soc. Jpn.* **44** 1405
[33] Jarczyk L, Kamys B, Kistryn M, Magiera A, Rudy Z, Strzalkowski A, Barna R, D'Amico V, De Pasquale D, Italiano A and Licandro M 1996 *Phys. Rev.* **C54** 1302
[34] CANAM URL `http://canam.ujf.cas.cz/`